



# Nanocomposites of epoxy-based shape memory polymer and thermally reduced graphite oxide: Mechanical, thermal and shape memory characterizations

Lei Chen <sup>a</sup>, Wenbing Li <sup>b</sup>, Yanju Liu <sup>a, \*\*</sup>, Jinsong Leng <sup>b, \*</sup>

<sup>a</sup> Department of Astronautical Science and Mechanics, Harbin Institute of Technology (HIT), P.O. Box 301, No. 92 West Dazhi Street, Harbin 150001, China

<sup>b</sup> Centre for Composite Materials and Structures, Science Park of Harbin Institute of Technology (HIT), P.O. Box 3011, No. 2 YiKuang Street, Harbin 150080, China

## ARTICLE INFO

### Article history:

Received 16 May 2015

Received in revised form

7 January 2016

Accepted 17 January 2016

Available online 3 February 2016

### Keywords:

A. Polymer-matrix composites (PMCs)

A. Smart materials

B. Interface/interphase

D. Mechanical testing

## ABSTRACT

Low mechanical strength and low thermal stability of pristine epoxy-based shape memory polymer (ESMP) hinder its practical applications, and the usually used reinforcing fillers are expensive. In this study, thermally reduced graphite oxide (TrGO) was used as a low-cost but efficient reinforcement phase for ESMP. Compared with pristine ESMP, an increase of 41%–71% for Young's modulus and 44%–64% for tensile strength were observed for the TrGO/ESMP composites containing only 1–3 wt.% TrGO. Thermogravimetric analysis (TGA) showed that 2 wt.% TrGO can improve the thermal stability of ESMP significantly. The thermal conductivity of TrGO/ESMP composites increased almost linearly with increasing TrGO content. Moreover, the TrGO/ESMP composite containing 2 wt.% TrGO can decrease the shape recovery time of ESMP down to 1 min as a result of enhanced thermal conductivity. The TrGO/ESMP composites with such improved properties may have great potential in smart systems.

© 2016 Elsevier Ltd. All rights reserved.

## 1. Introduction

Shape-memory polymers (SMPs) have the ability to recover their original shape from a temporary shape with stimulus such as heat, light, magnetism, moisture, change in pH, or electricity [1]. The shape memory mechanism is based on reversible energy conversion in polymer chain movement. Typically, when SMP is subject to heat and deformation and then cooled below its switch transition temperature, large internal stress can be stored in the cross-linking structure; by heating the SMP above its switch transition temperature, the SMP recovers its permanent shape by releasing the internal stress [2]. SMPs have several advantages over shape memory alloys, such as light weight, low cost, high shape deformability and recoverability, and tailor-able switch temperatures [3]. Based on these advantages, SMPs have many potential applications including clothing manufacturing, automobile engineering, and medical treatment [4]. However, pristine SMP materials suffer from relatively low thermal stability, low strength and

stiffness, which hinder their applications as functional and structural materials [5,6]. At room temperature, epoxy-based SMP (ESMP) shows an elastic modulus of about 1 GPa [7], styrene-based SMP (SSMP) has an elastic modulus of less than 1 GPa [8], while the elastic modulus of shape-memory polyurethane (SMPU) is only around 200 MPa [9,10].

Therefore, some reinforcing fillers are tried to improve the mechanical strength and thermal stability, while maintaining shape memory properties of pristine SMPs. These fillers include particles (such as SiC [11] and Fe<sub>3</sub>O<sub>4</sub> [12]), fibers (such as glass fibers [13], carbon fibers [6] and carbon nanotubes [14]), and sheets (such as graphene [15]). However, some of these fillers are expensive which limits their use in SMP composites (such as carbon nanotubes and graphene); while some additives need high weight fractions in the composites, but the improvements in some key properties of the SMP are not significant. For example, the recovery force of ESMP was increased by only 50% with 20 wt.% SiC [7], and that of SMPU was increased by only 20% with 1 wt.% nanoclay [10]. The mechanical, thermal and shape memory properties of SMP composites are determined by dispersion states of fillers and filler–polymer interactions [14]. Uniform dispersion of fillers and strong filler–polymer interactions result in improved thermal stabilization, mechanical and shape memory properties of the SMP

\* Corresponding author. Tel./fax: +86 451 86402328.

\*\* Corresponding author. Tel./fax: +86 451 86414825.

E-mail addresses: [yj\\_liu@hit.edu.cn](mailto:yj_liu@hit.edu.cn) (Y. Liu), [lengjs@hit.edu.cn](mailto:lengjs@hit.edu.cn) (J. Leng).

composites [14]. For ESMP, SMPU and shape-memory polyvinyl alcohol based composites, some polar groups (such as hydroxyl, carbonyl, and epoxy) on fillers can enhance the filler–matrix interfacial bonding, leading to significant improvements in mechanical properties [16,17], glass transition temperatures [18], and shape memory performances [19,20] of the SMP composites.

Thermally reduced graphite oxide (TrGO) is a kind of porous graphite material, which is synthesized by heating graphite oxide (GO) to 200–1100 °C [21,22] or treating GO with microwave [18]. Due to its high specific surface area (>100 m<sup>2</sup>/g) and large pore volume (>0.5 cm<sup>3</sup>/g) [23], high thermal [24] and electrical conductivity [25], strong mechanical property [26], polar surface [27] and fine compatibility with many polymers [28], TrGO has been widely used as reinforcement phase for high-performance polymer nanocomposites. The TrGO can significantly enhance the mechanical properties (such as tensile strength, Young's modulus, storage modulus, and hardness) of polyethylene [29], poly (methyl methacrylate) [30], polyvinyl alcohol [31], thermoplastic polyurethane [32], poly (ethylene oxide) [33], natural rubber [34], and many others [28]. Moreover, TrGO can improve thermal stability [32] and thermal conductivity [35] of polymers.

Because of the enormous surface area and surface polarity of TrGO, TrGO is believed to improve mechanical and thermal properties of ESMP. And some studies show that exfoliated GO materials, which have abundant oxygen-containing groups, show a good interfacial bonding with ESMP matrix [36,37]. In our previous study [38], 1 wt.% TrGO was incorporated into ESMP by three-roll mill (TRM), and the obtained TrGO/ESMP composite exhibited better mechanical property, higher thermal stability, and improved recovery force, compared with unfilled ESMP. Herein, different weight fractions of TrGO (1–3 wt.%) is incorporated into ESMP by TRM. The micro-structure, static mechanical property, glass transition, thermal stability and conductivity, and shape memory behavior of the TrGO/ESMP composites are systematically investigated as a function of TrGO content, and the optimized TrGO weight fraction in the TrGO/ESMP composites is discovered.

## 2. Experimental details

### 2.1. Materials

The graphite supplied by Sigma Aldrich had a particle size less than 20 μm. Concentrated sulfuric acid (H<sub>2</sub>SO<sub>4</sub>), sodium nitrate (NaNO<sub>3</sub>), potassium permanganate (KMnO<sub>4</sub>), hydrogen peroxide (H<sub>2</sub>O<sub>2</sub>), and hydrochloric acid (HCl) were of analytical grade and purchased from Sinopharm Chemical Reagent (Shanghai, China). ESMP resin in this study is a thermoset crosslinked network, consisting of epoxy resin, hardener, and linear epoxy monomer [39]. For curing, the resin was cast into a flat glass mold and cured at 80 °C for 1 h, then 150 °C for 6 h.

### 2.2. Preparation of TrGO/ESMP composites

The synthesis of TrGO can refer to [38]. TrGO/ESMP mixture pastes with different TrGO contents (1 wt.%, 2 wt.% and 3 wt.%, respectively) were prepared by a TRM device (EXAKT 80E, EXAKT Advanced Technologies GmbH, Germany) with gradually smaller gaps (from 100 μm down to 5 μm) between the rollers. After the combination of TrGO and ESMP resin, the paste was cast into a flat glass mold and cured at 80 °C for 1 h, followed by 150 °C for 6 h.

### 2.3. Characterization methods

Scanning electron microscope (SEM) analyses were performed with an environmental microscope (FEI-Quanta 200F). Before SEM

analysis, the samples were vacuum coated with a thin gold layer using a precision etching coating system (Model 682, Gatan, USA) and the duration was 10 min. X-ray diffraction (XRD) experiments were performed in a D/max-rb rotating anode X-ray diffractometer (Japan). Samples were scanned in the reflection mode using the Cu Kα 1 radiation (wavelength: 1.5405 Å). The tensile properties of the materials at 25 °C were measured according to the ASTM D638 test method using a materials testing machine (Z050, Zwick/Roell) with the following conditions: gage length, 25 mm; crosshead speed, 5 mm/min; load cell, 50 kN; and preload, 8 N. For flexural tests at 25 °C, the specimens with a dimension of 65 mm × 12.7 mm × 3 mm (according to ASTM-D790) were loaded in three-point bending until 25 mm at a rate of 1 mm/min with a support span of 48 mm on a universal testing machine (Zwick/Z010). For both tensile and flexural tests, more than five specimens were tested for each material. A dynamic mechanical analyzer (DMA/SDTA861, Mettler Toledo) in tension mode was used to measure the dynamic mechanical properties of pure ESMP and TrGO/ESMP composites. Scanning measurements were performed between 25 °C and 180 °C with 1 Hz at a heating rate of 10 °C/min. Thermogravimetric analysis (TGA) was conducted from 25 °C to 600 °C at a rate of 10 °C/min under 50 ml/min air flow (TGA/DSC 1, Mettler Toledo). Thermal conductivity tests were carried out by DRL-III heat conduction modulus testing instrument (Xiangke).

Shape memory test included five steps [38]. First step, cured samples were cut into strips (dimension: 50 mm × 3 mm × 3 mm), and five strips were prepared for each material. Second step, these strips were heated to 130 °C using a hot plate (MODELKW-4AH, CHEMAT TECHNOLOGY, INC.) and kept for 5 min. Third step, the heated samples were bent into U shapes around a mandrel with a radius of 5 mm. The maximum bending angle ( $\theta_{max}$ ) was 180°. Fourth step, the U-shaped samples were cooled down to 18 °C under external force. Then this force was removed and the deformed specimens were stored at 18 °C for 24 h. Last step, the fixed bending angles ( $\theta_f$ ) of the specimens were measured and then they were put onto the hot plate at 130 °C. The bending angle ( $\theta_i$ ) was recorded as a function of time since the beginning of heating. Shape fixity ratio ( $R_f$ ) was calculated by the equation:

$$R_f = \frac{\theta_f}{180^\circ} \times 100\% \quad (1)$$

Shape recovery ratio ( $R_r$ ) was calculated by the equation:

$$R_r = \frac{180^\circ - \theta_i}{180^\circ} \times 100\% \quad (2)$$

## 3. Results and discussion

### 3.1. Micro-structure characterization

The micro-structures of TrGO, pure ESMP and TrGO/ESMP composites were characterized using SEM and XRD methods, respectively. Fig. 1a shows SEM image of TrGO. The TrGO are layered (indicated by arrows 1 and 2) and porous (indicated by arrow 3) as a result of GO exfoliation [40]. This unique structure gives the TrGO a high Brunauer–Emmett–Teller (BET) specific surface area of about 300 m<sup>2</sup>/g, much higher than graphite [38]. The fracture surface of unfilled ESMP is very flat, as shown in Fig. 1b, which indicates a brittle fracture [41]. The particle on the fracture surface in Fig. 1b may come from specimen breakage, which reflects the smoothness of the fracture surface of pure ESMP. The fracture surfaces of TrGO/ESMP composites are rather rough (see Fig. 1c, d, and e) and the direction of crack propagation varies due to the existence of TrGO.

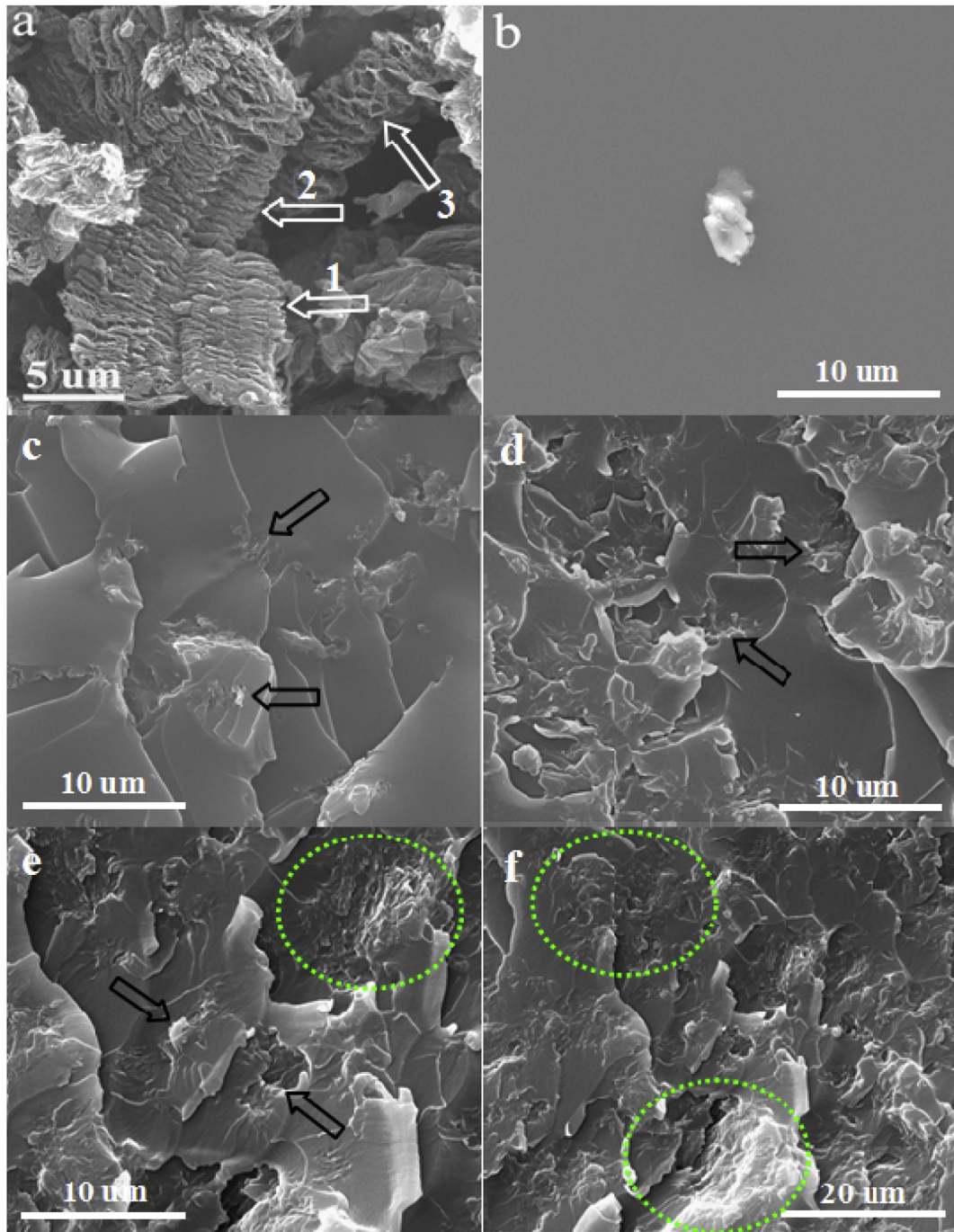


**Fig. 1.** SEM images of TrGO (a), pure ESMP (b), TrGO/ESMP composites with different TrGO contents: 1 wt.% (c), 2 wt.% (d), and 3 wt.% (e and f).

The roughness of the fracture surfaces might be an indication of crack distortion and hence, absorb more energy during fracture [42]. Furthermore, in all the TrGO/ESMP composites, the TrGO particles (indicated by black arrows) have an intimate contact with the matrix, which denotes a good interfacial adhesion between TrGO and ESMP. This results from the polar groups in TrGO (such as C=O, C–OH and COOH) which can promote the bonding between TrGO and ESMP [36,37]. Good compatibility due to the strong bonding can effectively prevent aggregation of TrGO in ESMP at low filler contents (1 wt.% and 2 wt.%). The uniform dispersion and good compatibility of TrGO in the ESMP may cause TrGO an efficient reinforcement to the ESMP. From a low-magnification SEM image of

the 3 wt.% TrGO/ESMP composite (Fig. 1f), a very dense TrGO network in the matrix is observed, and a few aggregations of TrGO are also found, as indicated by green circles. These aggregations would be negative for some properties of the composite, as will discussed later.

Fig. 2 shows the XRD patterns of TrGO, pure ESMP and TrGO/ESMP composites. Pure ESMP shows a wide peak at  $2\theta = 18^\circ$  corresponding to the scattering of cured epoxy molecules [43,44], which does not change after loading of TrGO. For the XRD pattern of TrGO, the wide and weak diffraction peak around  $23.5^\circ$  corresponds to the (002) graphitic plane of the graphite nanosheets in TrGO [43,44]. The low intensity of the (002) peak implies the



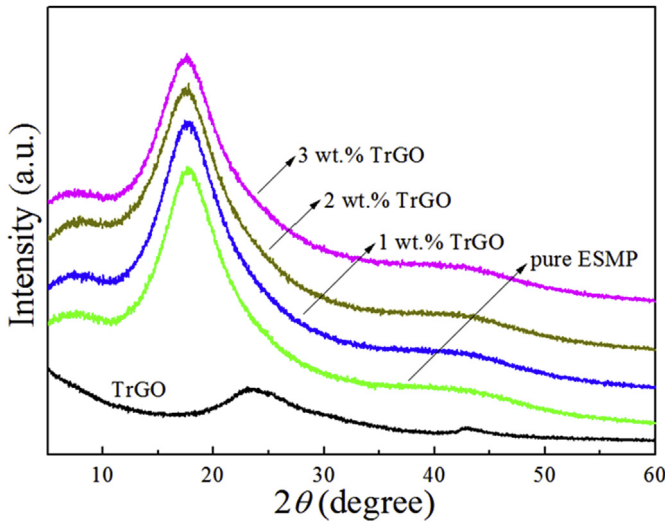


Fig. 2. XRD patterns for TrGO, pure ESMP and TrGO/ESMP composites with different TrGO contents.

graphite nanosheets have a very low number of graphitic layers [43]. After incorporation into ESMP, this diffraction peak disappears in all the TrGO/ESMP composites. This indicates the use of TRM during mixing TrGO and ESMP resin induced exfoliation of the graphite nanosheets in TrGO, leaving only very thin nanosheets which were unable to diffract [43,45].

### 3.2. Static mechanical properties

The static mechanical properties of pure ESMP and TrGO/ESMP composites were tested in terms of stress-strain and three-point bending behaviors at 25 °C. The representative tensile stress-strain curves are presented in Fig. 3a. For each case, the stress increased almost linearly with strain in the early stage. As shown in Fig. 3b, an increase of Young's modulus by 41%, 49% and 71% was obtained for the composite containing 1 wt.%, 2 wt.% and 3 wt.% TrGO, respectively. Similar to the Young's modulus, the tensile strength of the TrGO/ESMP composites were enhanced remarkably with the increasing TrGO content, as shown in Fig. 3c. An increase of tensile strength by 44%, 52% and 64% was observed for the composite containing 1 wt.%, 2 wt.% and 3 wt.% TrGO, respectively. A uniform dispersion of the TrGO and good interfacial interactions between TrGO and ESMP, as shown in Fig. 1, resulted in the improvement of Young's modulus and tensile strength of the composites [30,46]. However, the incorporation of TrGO lowered significantly the fracture elongation of ESMP, and the fracture elongation decreased with the increasing TrGO content, as shown in Fig. 3d. This was due to the strong molecular interactions between ESMP matrix and TrGO particles which reduced the ductility of the composites [47].

Fig. 4 displays the effect of TrGO content on the three-point bending properties of TrGO/ESMP composites. The typical load-deflection of midpoint curves are shown in Fig. 4a. The deflection of midpoint where fracture occurred decreased with increasing TrGO content. This indicates the TrGO in the ESMP prevents the polymer chains from free motions thus increasing the brittleness [48]. The bending modulus and bending strength are presented in Fig. 4b and c, respectively. Compared with pure ESMP, an increase of 20%, 60% and 123% in bending modulus and an improvement of 31%, 71% and 40% in bending strength were achieved for the composite containing 1 wt.%, 2 wt.% and 3 wt.% TrGO, respectively. The above results indicate the fine interfacial bonding between

TrGO and ESMP matrix is able to efficiently transmit stress from the matrix to the fillers.

### 3.3. Dynamic mechanical analysis (DMA)

Fig. 5a shows the storage modulus and  $\tan \delta$  of pure ESMP and TrGO/ESMP composites as a function of temperature. The overall storage modulus is higher for the composites compared with pure ESMP due to the reinforcement of TrGO [46,49]. The  $\tan \delta$  peak temperatures correspond to glass transition temperatures ( $T_g$ ) [50], which are compared in Fig. 5b. The  $T_g$  of pure ESMP is 98.2 °C, while the  $T_g$  for ESMP composites with 1 wt.% and 2 wt.% TrGO are 108.1 and 113.2 °C, respectively, indicating the TrGO can reduce the polymer chains freedom moving [51]. The ESMP composite with 3 wt.% TrGO has a  $T_g$  at 100.9 °C, which is lower than other TrGO/ESMP composites and is only 2.7 °C higher than pure ESMP. In the 3 wt.% TrGO/ESMP composite, the TrGO has a weak restriction on the polymer segments due to partial aggregation of TrGO, and so this composite has a  $T_g$  near pure ESMP [51,52].

### 3.4. Thermogravimetric analysis (TGA) and thermal conductivity measurements

The thermal degradation of pure ESMP and TrGO/ESMP composites were examined via TGA, as shown in Fig. 6a. For comparison, the degradation temperatures for 5% weight loss ( $T_{5\%}$ ) and the maximum weight loss rate ( $T_{max}$ ) were compared in Fig. 6b and c, respectively. The enhanced thermal stability of TrGO/ESMP composites (with 1 wt.% or 2 wt.% TrGO) originates from the barrier effect of TrGO to oxygen molecules [53]. The TrGO with a high specific surface area (about 300 m<sup>2</sup>/g [38]) can provide a barrier that prevents the movement of broken polymer chains, hinders the diffusion of volatile decomposition products and enhances char formation [54,55]. However, 3 wt.% TrGO adversely affects the thermal stability of ESMP. There may be two reasons. Firstly, because of partial aggregation of TrGO in the 3 wt.% TrGO/ESMP composite (see Fig. 1f), the TrGO in the ESMP matrix has a relatively weak barrier effect to oxygen. Secondly, because of high TrGO loading, the composite containing 3 wt.% TrGO has a higher thermal conductivity than pristine ESMP [56], as shown in Fig. 6d. The enhanced thermal conduction promoted thermal degradation of the composite, and thus this composite has a lower thermal stability than pure ESMP [57]. Fig. 6d also indicates the thermal conductivity of the TrGO/ESMP composite increases almost linearly with increasing TrGO contents, which will be beneficial for heat-triggered shape memory of the composites, as discussed in the next section.

### 3.5. Shape memory test of TrGO/ESMP composites

The most essential properties of SMPs and their composites are shape memory behaviors under external stimuli, such as heat [6,7,58]. The relationships between  $R_f$  and heating time during shape recovery of pure ESMP and TrGO/ESMP composite specimens are presented in Fig. 7, and the  $R_f$  and shape recovery times are summarized in Fig. 8. Fig. 7 shows all the specimens can recover totally ( $R_f = 100\%$ ) in 3 min. As shown in Fig. 8a, the TrGO-filled ESMP have higher  $R_f$  than pure ESMP, as a result of restricting effect of the TrGO on the polymer chain movements. Moreover, among the TrGO/ESMP composites, the composite containing 2 wt.% TrGO has the highest  $R_f$ , indicating the strongest restricting effect. As shown in Fig. 8b, both 1 wt.% and 3 wt.% TrGO increase the shape recovery time of ESMP, while 2 wt.% TrGO induces a shorter shape recovery time than unfilled ESMP. The shape recovery time is a result of competition between two main factors: filler-matrix

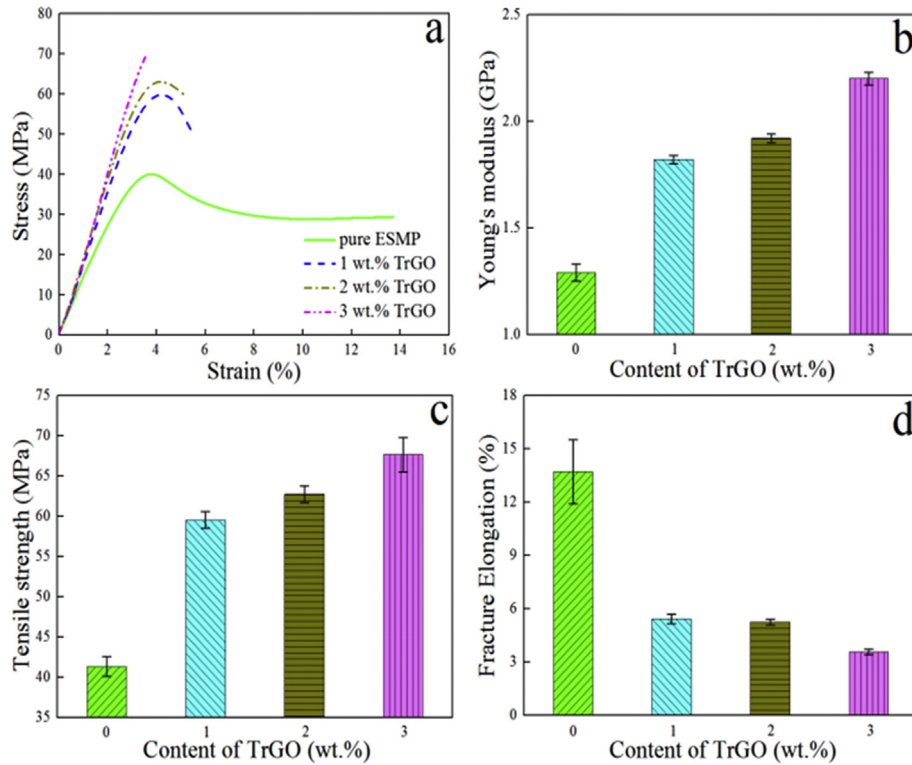


**Fig. 3.** Typical tensile stress-strain curves (a), Young's modulus (b), tensile strength (c) and fracture elongation (d) of pure ESMP and TrGO/ESMP composites with different TrGO contents measured at 25 °C.

interaction and thermal conductivity. In the case of the composite containing 1 wt.% TrGO that has a similar thermal conductivity to pristine ESMP, the uniformly dispersed TrGO particles can restrict

significantly the polymer chains from freedom moving; therefore, compared with pure ESMP, the polymer chains in this composite need a much longer time to reach their original positions when

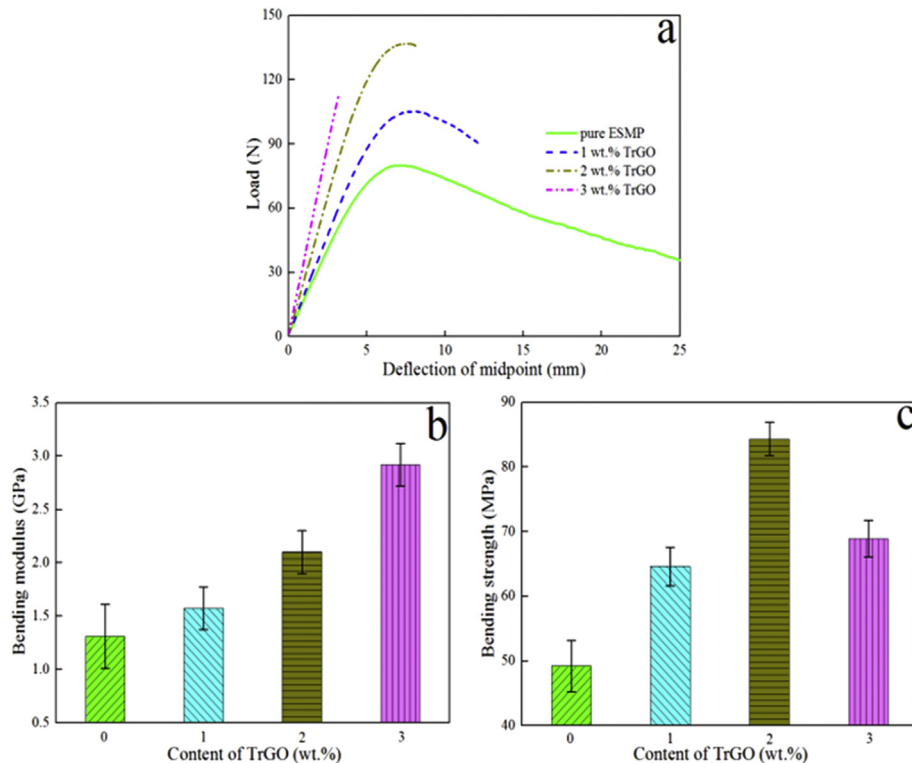


**Fig. 4.** (a) typical load-deflection of midpoint curves in three-point bending, (b) bending modulus and (c) bending strength of pure ESMP and TrGO/ESMP composites with different TrGO contents measured at 25 °C.

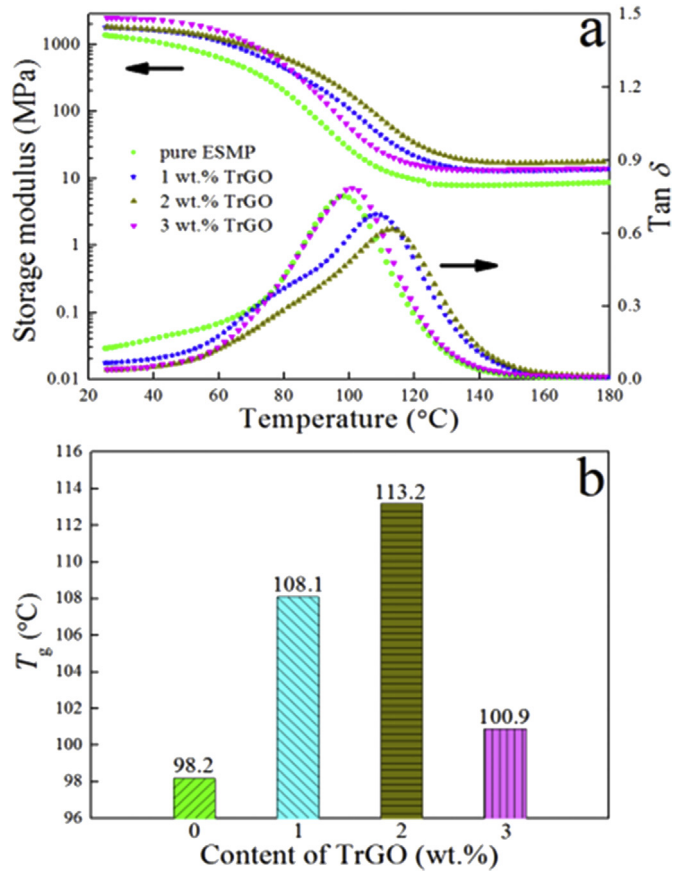


Fig. 5. (a) storage modulus and  $\tan \delta$  as a function of temperature, (b)  $T_g$  values of pure ESMP and TrGO/ESMP composites with different TrGO contents.

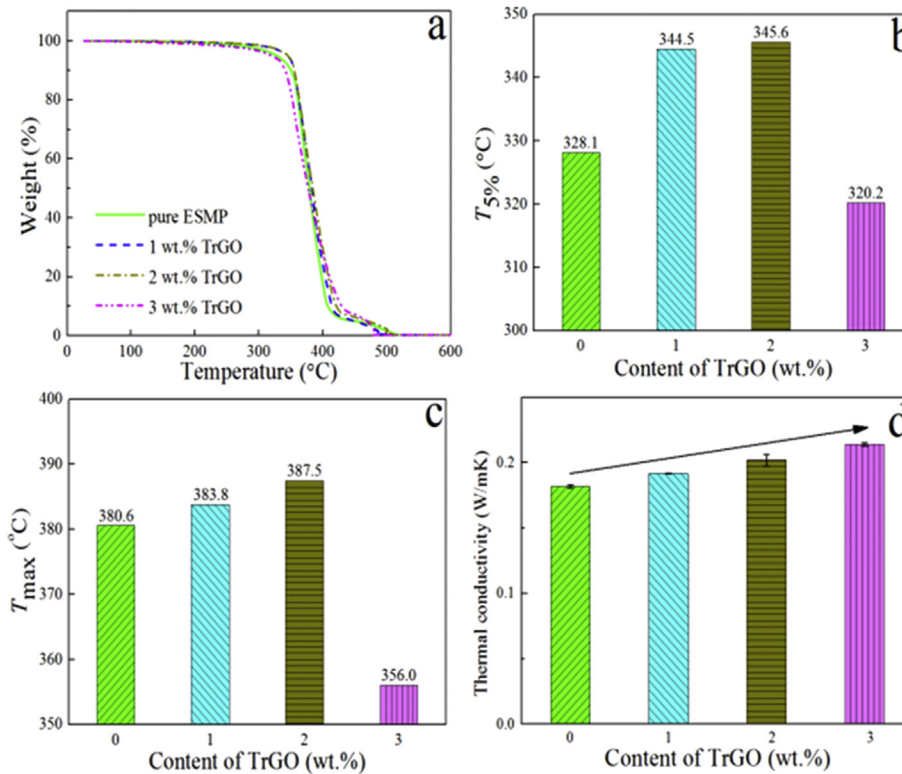


Fig. 6. (a) TGA curves, (b)  $T_{5\%}$ , (c)  $T_{max}$  and (d) thermal conductivities of pure ESMP and TrGO/ESMP composites with different TrGO contents.

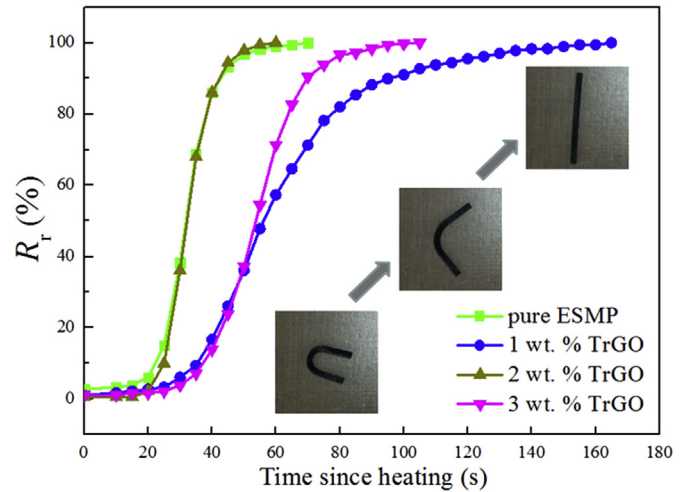


Fig. 7.  $R_r$  plotted as a function of heating time during free recovery of pure ESMP and TrGO/ESMP composites with different TrGO contents.

heated above its  $T_g$  temperature [38]. For the composite containing 2 wt.% TrGO, the uniformly dispersed TrGO particles can also restrict the freedom moving of polymer chains; however, it has a higher thermal conductivity than both pure ESMP and the composite with 1 wt.% TrGO (see Fig. 6d) which makes the composite's temperature to increase very quickly upon being heated on the hot plate. Thus the polymer chains move more faster than pure ESMP and the composite with 1 wt.% TrGO, leading to a shorter shape recovery time for the composite containing 2 wt.% TrGO. For the composite with 3 wt.% TrGO, although it has the highest thermal conductivity among the materials, the partial aggregation of TrGO

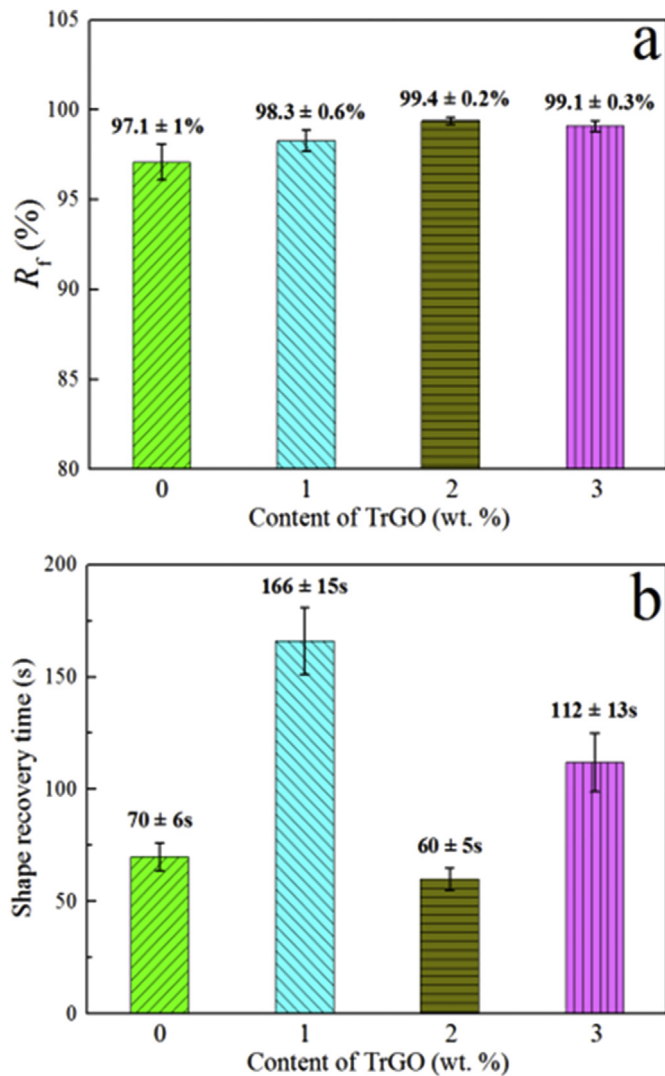


Fig. 8. Comparison of  $R_f$  values (a) and shape recovery times (b) of pure ESMP and TrGO/ESMP composites with different TrGO contents.

particles may lead to a waste of internal stored elastic strain energy during shape recovery [59], leading to a slower strain recovery and a longer shape recovery time compared with pure ESMP.

#### 4. Conclusions

In this study, porous and low-cost TrGO was used as reinforcement filler for ESMP. The micro-structures, mechanical and thermal properties, and shape memory behaviors of the TrGO/ESMP composites were examined as a function of TrGO contents. SEM photographs demonstrated that the TrGO particles were dispersed uniformly in the ESMP matrix, though a few aggregations were observed at 3 wt.% TrGO loading. Static mechanical tests indicated the Young's modulus, tensile strength, bending modulus and bending strength of ESMP were improved significantly by adding TrGO. The thermal stability of ESMP was improved by 1 wt.% or 2 wt.% TrGO, whereas 3 wt.% TrGO lowered its thermal stability in air condition. The  $R_f$  of ESMP was increased slightly by adding TrGO, and 2 wt.% TrGO was proven to give a faster shape recovery than unfilled ESMP. Considering the mechanical property, thermal stability and shape memory behavior (including shape recovery time

and  $R_f$ ) of the TrGO/ESMP composites, the optimum TrGO content should be 2 wt.%.

#### Acknowledgments

This work is supported by the National Natural Science Foundation of China (Grant No.11225211), for which we are very grateful.

#### References

- [1] Leng JS, Lan X, Liu YJ, Du SY. Shape-memory polymers and their composites: stimulus methods and applications. *Prog Mater Sci* 2011;56(7):1077–135.
- [2] Behl M, Lendlein A. Shape-memory polymers. *Mater Today* 2007;10(4):20–8.
- [3] Lendlein A, Jiang H, Junger O, Langer R. Light induced shape memory polymers. *Nature* 2005;434:879–82.
- [4] Meng QH, Hu JL. A review of shape memory polymer composites and blends. *Compos Part A Appl S* 2009;40(11):1661–72.
- [5] Lan X, Liu YJ, Lv HB, Wang XH, Leng JS, Du SY. Fiber reinforced shape-memory polymer composite and its application in a deployable hinge. *Smart Mater Struct* 2009;18(2):024002.
- [6] Gall K, Mikulas M, Munshi NA, Beavers F, Tupper M. Carbon fiber reinforced shape memory polymer composites. *J Intell Mater Syst Struct* 2000;11(11):877–86.
- [7] Gall K, Dunn ML, Liu Y, Finch D, Lake M, Munshi NA. Shape memory polymer nanocomposites. *Acta Mater* 2002;50(20):5115–26.
- [8] Tandon GP, Goecke K, Cable K, Baur J. Durability assessment of styrene- and epoxy-based shape-memory polymer resins. *J Intell Mater Syst Struct* 2009;20(17):2127–43.
- [9] Gunes IS, Cao F, Jana SC. Evaluation of nanoparticulate fillers for development of shape memory polyurethane nanocomposites. *Polymer* 2008;49(9):2223–34.
- [10] Cao F, Jana SC. Nanoclay-tethered shape memory polyurethane nanocomposites. *Polymer* 2007;48(13):3790–800.
- [11] Liu Y, Gall K, Dunn ML, McCluskey P. Thermomechanics of shape memory polymer nanocomposites. *Mech Mater* 2004;36(10):929–40.
- [12] Kalita H, Karak N. Bio-based hyperbranched polyurethane/Fe<sub>3</sub>O<sub>4</sub> nanocomposites as shape memory materials. *Polym Adv Technol* 2013;24(9):819–23.
- [13] Ohki T, Ni QQ, Ohsako N, Iwamoto M. Mechanical and shape memory behavior of composites with shape memory polymer. *Compos Part A Appl S* 2004;35(9):1065–73.
- [14] Rana S, Karak N, Cho JW, Kim YH. Enhanced dispersion of carbon nanotubes in hyperbranched polyurethane and properties of nanocomposites. *Nanotechnology* 2008;19(49):495707.
- [15] Jung YC, Kim JH, Hayashi T, Kim YA, Endo M, Terrones M, et al. Fabrication of transparent, tough, and conductive shape-memory polyurethane films by incorporating a small amount of high-quality graphene. *Macromol Rapid Commun* 2012;33(8):628–34.
- [16] Martin-Gallego M, Bernal MM, Hernandez M, Verdejo R, Lopez-Manchado MA. Comparison of filler percolation and mechanical properties in graphene and carbon nanotubes filled epoxy nanocomposites. *Eur Polym J* 2013;49(6):1347–53.
- [17] Pokharel P, Pant B, Pokhrel K, Pant HR, Lim JG, Lee DS, et al. Effects of functional groups on the graphene sheet for improving the thermomechanical properties of polyurethane nanocomposites. *Compos Part B Eng* 2015;78:192–201.
- [18] Pokharel P, Truong QT, Lee DS. Multi-step microwave reduction of graphite oxide and its use in the formation of electrically conductive graphene/epoxy composites. *Compos Part B Eng* 2014;64:187–93.
- [19] Gu S, Yan B, Liu L, Ren J. Carbon nanotube-polyurethane shape memory nanocomposites with low trigger temperature. *Eur Polym J* 2013;49(12):3867–77.
- [20] Du FP, Ye EZ, Tang CY, Ng SP, Zhou XP, Xie XL. Microstructure and shape memory effect of acidic carbon nanotubes reinforced polyvinyl alcohol nanocomposites. *J Appl Polym Sci* 2013;129(3):1299–305.
- [21] Sun G, Zheng L, Zhan Z, Zhou J, Liu X, Li L. Actuation triggered exfoliation of graphene oxide at low temperature for electrochemical capacitor applications. *Carbon* 2014;68:748–54.
- [22] Schniepp HC, Li JL, McAllister MJ, Sai H, Herrera-Alonso M, Adamson DH, et al. Functionalized single graphene sheets derived from splitting graphite oxide. *J Phys Chem B* 2006;110(17):8535–9.
- [23] Yang SJ, Kim T, Jung H, Park CR. The effect of heating rate on porosity production during the low temperature reduction of graphite oxide. *Carbon* 2013;53:73–80.
- [24] Teng CC, Ma CCM, Lu CH, Yang SY, Lee SH, Hsiao MC, et al. Thermal conductivity and structure of non-covalent functionalized graphene/epoxy composites. *Carbon* 2011;49:5107–16.
- [25] Kim H, Miura Y, Macosko CW. Graphene/polyurethane nanocomposites for improved gas barrier and electrical conductivity. *Chem Mater* 2010;22(11):3441–50.



- [26] Rafiee MA, Rafiee J, Wang Z, Song H, Yu ZZ, Koratkar N. Enhanced mechanical properties of nanocomposites at low graphene content. *ACS Nano* 2009;3(12): 3884–90.
- [27] Zhang C, Lv W, Xie X, Tang D, Liu C, Yang QH. Towards low temperature thermal exfoliation of graphite oxide for graphene production. *Carbon* 2013;62:11–24.
- [28] Steurer P, Wissert R, Thomann R, Mülhaupt R. Functionalized graphenes and thermoplastic nanocomposites based upon expanded graphite oxide. *Macromol Rapid Commun* 2009;30(4–5):316–27.
- [29] Todd AD, Bielawski CW. Thermally reduced graphite oxide reinforced polyethylene composites: a mild synthetic approach. *Polymer* 2013;54(17):4427–30.
- [30] Ji WF, Chang KC, Lai MC, Li CW, Hsu SC, Chuang TL, et al. Preparation and comparison of the physical properties of PMMA/thermally reduced graphene oxides composites with different carboxylic group content of thermally reduced graphene oxides. *Compos Part A Appl S* 2014;65:108–14.
- [31] Das B, Prasad KE, Ramamurthy U, Rao CNR. Nano-indentation studies on polymer matrix composites reinforced by few-layer graphene. *Nanotechnology* 2009;20(12):125705.
- [32] Bian J, Lin HL, He FX, Wei XW, Chang IT, Sancaktar E. Fabrication of microwave exfoliated graphite oxide reinforced thermoplastic polyurethane nanocomposites: effects of filler on morphology, mechanical, thermal and conductive properties. *Compos Part A Appl S* 2013;47:72–82.
- [33] Lee HB, Raghu AV, Yoon KS, Jeong HM. Preparation and characterization of poly(ethylene oxide)/graphene nanocomposites from an aqueous medium. *J Macromol Sci B* 2010;49(4):802–9.
- [34] Potts JR, Shankar O, Murali S, Du L, Ruoff RS. Latex and two-roll mill processing of thermally-exfoliated graphite oxide/natural rubber nanocomposites. *Compos Sci Technol* 2013;74:166–72.
- [35] Shi JN, Ger MD, Liu YM, Fan YC, Wen NT, Lin CK, et al. Improving the thermal conductivity and shape-stabilization of phase change materials using nano-graphite additives. *Carbon* 2013;51:365–72.
- [36] Lu H, Yao Y, Huang WM, Hui D. Noncovalently functionalized carbon fiber by grafted self-assembled graphene oxide and the synergistic effect on polymeric shape memory nanocomposites. *Compos Part B Eng* 2014;67:290–5.
- [37] Lu H, Liang F, Gou J, Leng J, Du S. Synergistic effect of Ag nanoparticle-decorated graphene oxide and carbon fiber on electrical actuation of polymeric shape memory nanocomposites. *Smart Mater Struct* 2014;23:085034.
- [38] Chen L, Li WB, Liu YJ, Leng JS. Epoxy shape-memory polymer reinforced by thermally reduced graphite oxide: influence of processing techniques. *J Appl Polym Sci* 2015;132(38):42502.
- [39] Leng JS, Wu XL, Liu YJ. Effect of a linear monomer on the thermomechanical properties of epoxy shape-memory polymer. *Smart Mater Struct* 2009;18(9): 095031.
- [40] Kaniyoor A, Baby TT, Arockiadoss T, Rajalakshmi N, Ramaprabhu S. Wrinkled graphenes: a study on the effects of synthesis parameters on exfoliation-reduction of graphite oxide. *J Phys Chem C* 2011;115(36):17660–9.
- [41] Zhao LM, Feng X, Li YF, Mi XJ. Shape memory effect and mechanical properties of graphene/epoxy composites. *Polym Sci Ser A+* 2014;56(5):640–5.
- [42] Goyal RK, Samant SD, Thakar AK, Kadam A. Electrical properties of polymer/expanded graphite nanocomposites with low percolation. *J Phys D Appl Phys* 2010;43:365404.
- [43] Prolongo SG, Jimenez-Suarez A, Moriche R, Ureña A. In situ processing of epoxy composites reinforced with graphene nanoplatelets. *Compos Sci Technol* 2013;86:185–91.
- [44] Zaman I, Kuan HC, Meng Q, Michelmoro A, Kawashima N, Pitt T, et al. A facile approach to chemically modified graphene and its polymer nanocomposites. *Adv Funct Mater* 2012;22(13):2735–43.
- [45] Yasmin A, Luo JJ, Daniel IM. Processing of expanded graphite reinforced polymer nanocomposites. *Compos Sci Technol* 2006;66(9):1179–86.
- [46] Tang LC, Wan YJ, Yan D, Pei YB, Zhao L, Li YB, et al. The effect of graphene dispersion on the mechanical properties of graphene/epoxy composites. *Carbon* 2013;60:16–27.
- [47] Gan L, Shang SM, Yuen CWM, Jiang SX, Luo NM. Facile preparation of graphene nanoribbon filled silicone rubber nanocomposite with improved thermal and mechanical properties. *Compos Part B Eng* 2015;69:237–42.
- [48] Rezanejad S, Kokabi M. Shape memory and mechanical properties of cross-linked polyethylene/clay nanocomposites. *Eur Polym J* 2007;43(7):2856–65.
- [49] Zhang X, Wang J, Jia H, You S, Xiong X, Ding L, et al. Multifunctional nanocomposites between natural rubber and polyvinyl pyrrolidone modified graphene. *Compos Part B Eng* 2016;84:121–9.
- [50] Castro F, Westbrook KK, Hermiller J, Ahn DU, Ding YF, Qi HJ. Time and temperature dependent recovery of epoxy-based shape memory polymers. *J Eng Mater-T ASME* 2011;133:021025.
- [51] Du FP, Ye EZ, Yang W, Shen TH, Tang CY, Xie XL, et al. Electroactive shape memory polymer based on optimized multi-walled carbon nanotubes/polyvinyl alcohol nanocomposites. *Compos Part B Eng* 2015;68:170–5.
- [52] Pongsa U, Somwangthanoj A. Effective thermal conductivity of 3,5-diaminobenzoyl-functionalized multiwalled carbon nanotubes/epoxy composites. *J Appl Polym Sci* 2013;130(5):3184–96.
- [53] Jeon GW, An JE, Jeong YG. High performance cellulose acetate propionate composites reinforced with exfoliated graphene. *Compos Part B Eng* 2012;43(8):3412–8.
- [54] Nguyen DA, Lee YR, Raghu AV, Jeong HM, Shin CM, Kim BK. Morphological and physical properties of a thermoplastic polyurethane reinforced with functionalized graphene sheet. *Polym Int* 2009;58:412–7.
- [55] Zhao YH, Zhang YF, Wu ZK, Bai SL. Synergic enhancement of thermal properties of polymer composites by graphene foam and carbon black. *Compos Part B Eng* 2016;84:52–8.
- [56] Teng CC, Ma CCM, Lu CH, Yang SY, Lee SH, Hsiao MC, et al. Thermal conductivity and structure of non-covalent functionalized graphene/epoxy composites. *Carbon* 2011;49(15):5107–16.
- [57] Lee YR, Raghu AV, Jeong HM, Kim BK. Properties of waterborne polyurethane/functionalized graphene sheet nanocomposites prepared by an in situ method. *Macromol Chem Phys* 2009;210(15):1247–54.
- [58] Yakacki CM, Shandas R, Lanning C, Rech B, Eckstein A, Gall K. Unconstrained recovery characterization of shape-memory polymer networks for cardiovascular applications. *Biomaterials* 2007;28(14):2255–63.
- [59] Ni QQ, Zhang C, Fu Y, Dai G, Kimura T. Shape memory effect and mechanical properties of carbon nanotube/shape memory polymer nanocomposites. *Compos Struct* 2007;81(2):176–84.